Pergamon

Int. J. Heat Mass Transfer. Vol. 38, No. 17, pp. 3263–3273, 1995

0017-9310/95 $9.50+0.00

0017-9310(95)00058-5

Unsteady heat transfer and particle behavior around a horizontal tube bundle near an expanded bed surface of a gas fluidized bed: conditional sampling statistical analysis

M. MIYAMOTO, K. TAKAHASHI, JIN REN JIE, Y. KATOH and J. KURIMA
Department of Mechanical Engineering, Yamaguchi University, Tokiwadai, Ube, 755, Japan

(*Received* 1 *June* 1994 *and in final form* 4 *January* 1995)

Abstract—The heat transfer augmentation by particles making contact with a heat transfer surface in a fluidized bed was studied. The instantaneous local heat transfer coefficient and particle packing around the tube were simultaneously measured at the same location. The measured results were analysed by the conditional averaging method, distinguishing between particle contact and no particle contact. The average local heat transfer coefficient in the periods during particle contact can be closely correlated by an exponential function of the average local particle packing.

1. INTRODUCTION

There are many unknown details in the heat transfer mechanism around horizontal tubes in a fluidized bed. Several mechanistic models of heat transfer in fluidized beds have been developed by many investigators, and the trends of the experimental results on the average heat transfer coefficient might be quite well explained using these models [1]. Recently instantaneous local heat transfer coefficients have also been measured by many investigators [2–5], but to evaluate accurately the augmentations of the heat transfer rate that resulted from particles making contact with the heat transfer surface, not only the instantaneous local heat transfer coefficients but also the particle behavior on the heat transfer surface should be simultaneously measured. Therefore, it cannot be stated that the experimental measurements from these aspects have been thoroughly performed or that the heat transfer mechanisms have been made clear. Especially near the expanded bed surface of a fluidized bed, the particles are violently agitated. This state of fluidization, which was mainly investigated in the present study, cannot be accurately evaluated using the simplified two-phase model of the emulsion and bubble phases [6]. Consequently, the heat transfer mechanisms around the tube in such a condition have not been clarified.

In the present study, the instantaneous local heat transfer coefficients and the particle behavior were simultaneously measured at the same location on a horizontal tube in a fluidized bed with glass beads with an average diameter of 0.42 mm. In the present measurements, the methods used in the previous study [7] were improved to make the frequency response higher. The measured results were statistically analysed, using the conditional averaging method, by which the period when the particles were making contact with the tube surface could be distinguished from the period of no particle contact, in order to make the mechanisms of the heat transfer augmentation resulting from the particle contact clear.

2. EXPERIMENTAL APPARATUS AND MEASURING METHOD

The cold model fluidized bed with a 400 mm × 400 mm cross-section and a tube bundle of two-vertical-row staggered horizontal tubes (with diameter 34 mm) used in the present study is shown in Fig. 1. A single cylinder designated as the heated tube in Fig. 1 is the instrumented heat transfer tube. The distributor plate was a punched plate with an open area ratio of 4%. The bulk temperature of the bed, T_b was measured by a sheathed thermocouple with a diameter of 2.2 mm at the bed center, located 50 mm above the distributor. Glass beads, with an average diameter of 0.42 mm, solid density of 2490 kg m^{-3} and bulk density of 1580 kg m^{-3}, were used as the fluidized particles. Their measured minimum fluidization velocity, U_{mf}, was 0.14 m s^{-1}.

The instrumented cylinder is shown in Fig. 2. A stainless steel foil with a thickness of 0.012 mm was stuck around a polycarbonate circular cylinder with adhesive tape (thickness of 0.127 mm). The foil was uniformly heated by a direct electrical current. As shown in Fig. 2, to detect the particle behavior, two optical probes with parallel alignment were constructed from four optical fibers (each with a diameter of 0.5 mm), which were stuck to the surface of the foil in straight lines parallel to the tube axis. There were LED lights on the tips of two fibers on the left-hand

NOMENCLATURE

d_p average particle diameter
H instantaneous local heat transfer coefficient, equation (2)
H_a overall time-average local heat transfer coefficient
H_b time-average local heat transfer coefficient during no particle contact
H_p time-average local heat transfer coefficient during particle contact
L_b, L_s average height of expanded bed surface and static bed height
N number of particles existing in detecting space of optical probe
Nu_{ba} circumferential average of time-average local Nusselt number ($= H_b d_p/\lambda$) during no particle contact
Nu_p time-average local Nusselt number during particle contact, $H_p d_p/\lambda$
q_s, q_w surface heat flux and heat-generation rate per unit surface area
Re_m Reynolds number, $U_m d_p/\nu$
R_p time fraction of periods during particle contact
T_b bulk temperature of bed
T_c, T_s thermocouple temperature and surface temperature
U_0, U_d superficial gas velocity and excess gas velocity, $U_0 - U_{mf}$
U_m maximum velocity of gas through tube bundle
U_{mf} minimum fluidization velocity
V_c circumferential velocity of particle (being negative in the clockwise direction)
V_p normalized output of optical fiber probe.

Greek symbols
ε void fraction defined by equation (1)
$1-\varepsilon'$ normalized local particle packing, equation (1)
$(1-\varepsilon')_p$ normalized local particle packing averaged during particle contact
θ azimuthal angle measured from bottom of tube in the clockwise direction
λ thermal conductivity of air
ν kinematic viscosity of air
τ time.

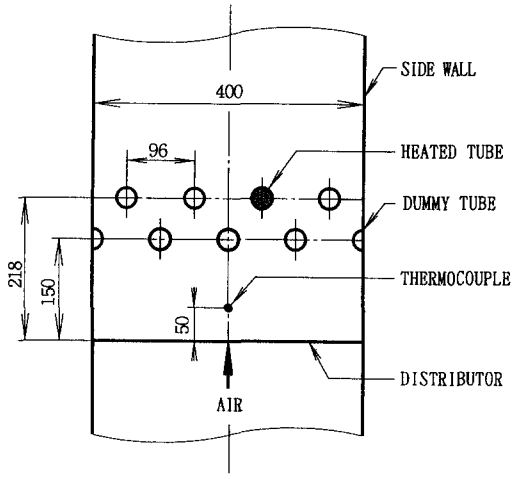

Fig. 1. Experimental fluidized bed. (Units in mm.)

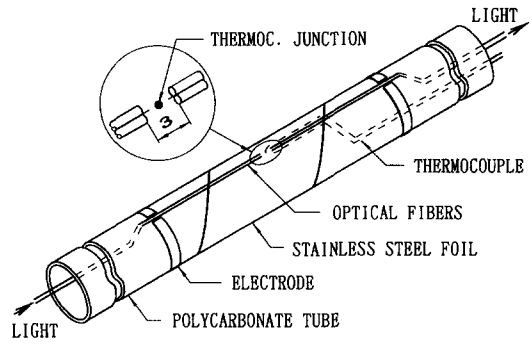

Fig. 2. Instrumented cylinder. (Units in mm.)

side and the light from them was attenuated by the existing particles and then received by the other two fibers on the right-hand side. The distance between the facing tips of fibers was 3 mm. A chromel–constantan thermocouple with a diameter of 0.012 mm was inserted between the foil and the adhesive tape, and its junction was located at the center of the 3 mm interval between the facing tips of fibers. The instrumented cylinder was allowed to rotate to change the azimuthal angle of the measuring point. It was experimentally confirmed that the distributions of the time-average heat transfer coefficient around tube were generally unchanged by the effects of projection formed by the optical fibers on the cylinder.

The light signals received by the two fibers were converted to voltage signals by photodiode modules, amplified and transmitted to a personal computer after A/D conversion (12 bit) and then saved on magnetic optical disks, along with the outputs from the thermocouples. The measurements were carried out at a sampling rate of 1 kHz and a sampling time of about 60 s for each run (only for the particle velocity measurement, the sampling rate and time were 10 kHz and about 60 s respectively).

In the present study, the static bed heights, L_s, were 100, 150 and 200 mm, and for each L_s, the superficial

Table 1. Average height of expanded bed surface

L_s (mm)	L_b (mm)				
	$U_d = 0.30$ m s^{-1}	0.50	0.70	0.90	1.10
100	×	120–160	145–165	165–180	170–190
150	×	195–215	220–230	240–250	×
200	240–250	260–270	260–280	270–290	×

gas velocities, U_0, were 0.64, 0.84 and 1.04 m s^{-1}. U_0 of 1.24 m s^{-1} was added for L_s of 100 mm, and U_0 of 0.44 m s^{-1} was added for L_s of 200 mm. The present experimental conditions were in the bubbling flow regime and the formation of bubbles was always able to be observed. The average height, L_b, of the expanded bed surface from the distributor, which was observed in the present experimental conditions, is given in Table 1. The height of the center line of the heat transfer tube was 218 mm. The average heights of the expanded bed surface located below, near and above the heat transfer tube for L_s = 100, 150 and 200 mm, respectively, are also shown in Table 1.

3. ESTIMATION OF INSTANTANEOUS LOCAL HEAT TRANSFER COEFFICIENTS

The inverse heat conduction analysis method proposed by Beck *et al.* [8] was used to calculate the instantaneous local heat transfer coefficients from the temperatures measured by the inserted thermocouple. An unsteady heat conduction in a composite body that was composed of the stainless steel foil, adhesive tape, polycarbonate cylinder and thermocouple was numerically analysed by an approximate one-dimensional heat conduction model including two unknown parameters, which were the exact location of the thermocouple junction and the thermal resistance between the thermocouple and its surrounding medium. To determine these unknowns, when the stainless steel foil was heated by a step change of electrical current, the temperature change of the thermocouple was measured and compared with the finite-difference solutions obtained by the present one-dimensional heat conduction model with the heat input of the measured heat generation rate, q_w. In Fig. 3, the measured temperatures, T_c, of the thermocouple

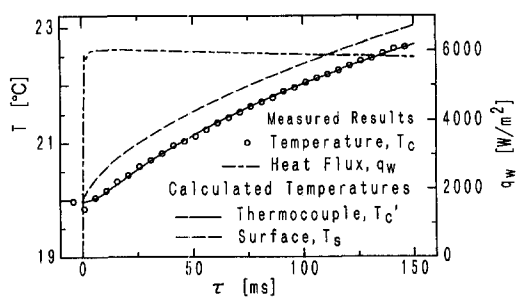

Fig. 3. Comparisons of calculated temperature, T_c' with measured temperature, T_c.

are compared with the numerical solutions, T_c', calculated using the estimated values of the unknown parameters. It is shown in Fig. 3 that the compared temperatures agree very well and the temperature change of thermocouple has a time lag behind the surface temperature change, T_s.

In the present inverse heat conduction analysis, the time increment was 1 ms, and the temperature and heat flux at the surface were calculated from the measured temperatures at eight future time steps (R = 9 [8]). The frequency response of the present measuring system to a square-wave change of heat transfer coefficient was checked using a numerical simulation. This simulation showed that the amplitude of the calculated heat transfer coefficient was attenuated to 75% of the one given with a square-wave change at frequency of 40 Hz and was attenuated to 50% at 50 Hz. George [4] pointed out that in order to accurately measure the instantaneous local heat transfer coefficients in the fluidized bed of glass beads with a diameter of 1 mm, the measuring system should respond accurately to surface heat flux fluctuations as rapid as 100 Hz. However, his results also show that the main part of the frequency spectra of the fluctuating heat transfer coefficients is lower than 40 Hz. Therefore, the present measuring system may be considered to have sufficient frequency response unless the minimum and maximum values themselves of instantaneous heat transfer coefficients are to be determined.

4. ESTIMATION OF PARTICLE PACKING AND PARTICLE VELOCITY

The method of estimating the particle packing in the space between the facing tips of four optical fibers is similar to that of the previous study [7]. The glass beads used in the present study are transparent and have a refractivity of 1.52. Therefore, even when the detecting space between the facing tips is fully packed, some light can be transmitted through that space. This fact means that the present optical probes can correctly detect the particle packing over a wide range from the dilute condition to the dense phase. The voltage outputs from the two optical probes, each of which was composed of a pair of fibers with facing tips, were normalized with their own values of the maximum and minimum outputs. The particle packing in the detecting space was determined from the arithmetic means of the two normalized outputs, using

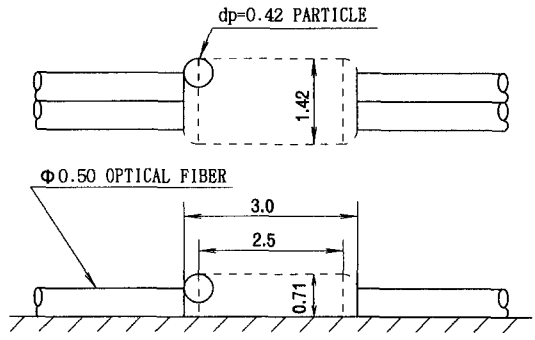

Fig. 4. Detecting volume of optical probe system. (Units in mm.)

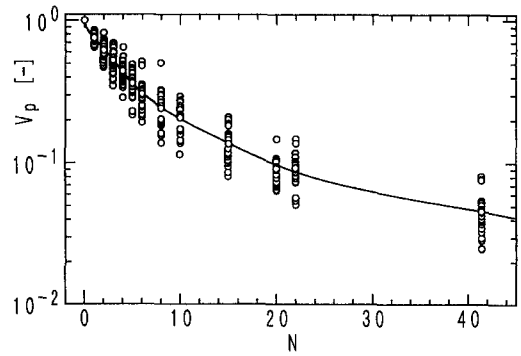

Fig. 5. Relation between normalized optical probe output, V_p, and number of particles, N, in detecting space of optical probe system

the relation between the particle packing and the optical probe output obtained from preparatory experiments.

The volume of the detecting space between the facing tips of the fibers is shown in Fig. 4. In Fig. 5, the normalized outputs from the optical probe system are plotted against the number, N, of the particles in the detecting space. The plotted data in Fig. 5 were obtained by the preparatory measurements, in which the same optical probe system was constructed on a flat plate instead of on the cylinder in order to be able to easily place the glass beads in the detecting space. The solid line indicates the average of the plotted data and gives the relation used to calculate the local particle packing on the surface from the optical probe outputs in the present study. In the experimental bed, the probability that V_p takes extreme values (i.e. different from the average value) is considered to be lower than that of V_p being found adjacent to the solid line. The number of particles existing in the detecting volume is related to the normalized values of the particle packing, $(1-\varepsilon')$, as shown in the following equation

$$(1-\varepsilon') = \frac{(1-\varepsilon)}{(1-\varepsilon)_{max}} = \frac{N}{N_{max}} \quad (1)$$

where N_{max} is the maximum number of particles in the detecting volume and $(1-\varepsilon)_{max}$ is the maximum of $(1-\varepsilon)$, corresponding to the emulsion phase with bulk density of 1580 kg m^{-3}. In the present experimental conditions, $N_{max} = 41.4$ and $(1-\varepsilon)_{max} = 0.632$.

Furthermore, the circumferential velocity of particles on the heat transfer tube was estimated by measuring the time required for the particles to travel between the two optical probes. The cross-correlation coefficients between the output signals from two optical probes were calculated, putting the various time displacements between these two signals. The particle traveling time was equal to the time displacement that maximized the cross-correlation coefficients [9]. But the optical fiber arrangement and the sampling frequency used in the present experiments were not necessarily well fitted to the particle velocity measurement, because in the present study the measurements of particle packing were made prior to the measurements of the particle velocity. Consequently, the measured particle velocities were used only to qualitatively grasp the particle movement. The particle velocities were determined at intervals of 10 ms. Then, for the cases of $L_s = 100$ and 150 mm, the cross-correlation coefficients at each interval were computed using 500 data (with sampling frequency of 10 kHz) from each optical probe, and 1000 data were used for $L_s = 200$ mm.

5. EXPERIMENTAL RESULTS AND DISCUSSION

The measurements of heat transfer coefficients and particle packing were carried out at nine angular positions of the heat transfer tube from the bottom, $\theta = 0°$, to the top, $\theta = 180°$, at intervals of 22.5° by rotating the tube in the clockwise direction. The particle velocities were measured at intervals of 45°.

Figure 6 shows typical examples of the measured results at $\theta = 0°$, 90° and 180° for $L_s = 100$, 150 and 200 mm, when the excess gas velocity, U_d is 0.7 m s^{-1}. In Fig. 6, the instantaneous local heat transfer coefficients for H, the normalized particle packing, $(1-\varepsilon')$ and the circumferential particle sliding velocities, V_c, on the instrumented cylinder are shown for 3 s duration along with the measured thermocouple temperatures, T_c. The particle velocity in the counterclockwise direction was taken to be positive. As shown in Table 1, the average heights of the expanded bed surface for L_s of 100, 150 and 200 mm were below, near and above the center line height of the heat transfer tube respectively. The instantaneous local heat transfer coefficient, H is defined by the following equation.

$$H = \frac{q_s}{T_s - T_b}. \quad (2)$$

For L_s of 100 mm, generally, the particles do not come into frequent contact with the heat transfer surface. At the bottom of the tube, the particle-packet contacts take place occasionally and make the corresponding heat transfer coefficient higher. The dur-

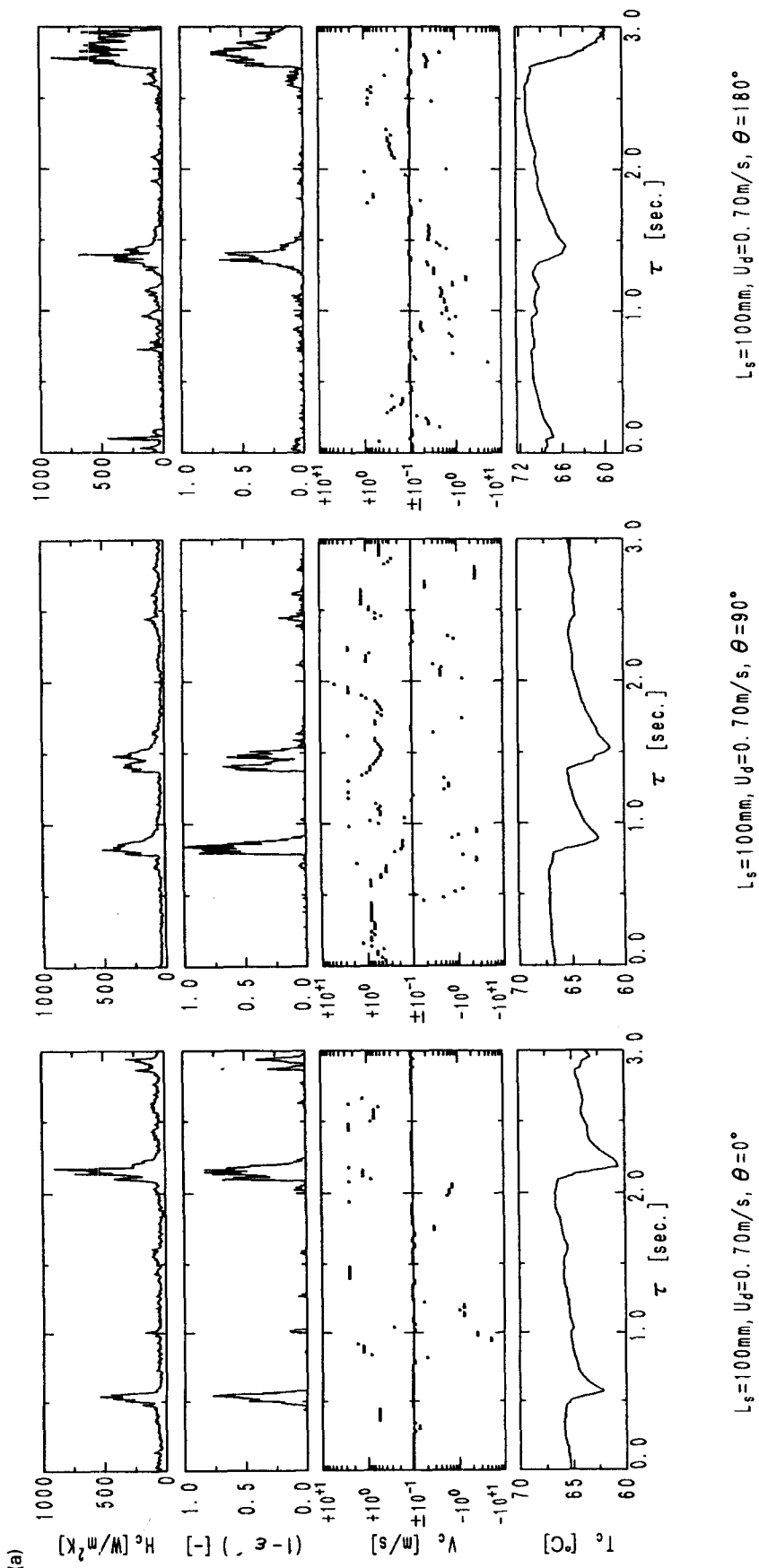

Fig. 6. Instantaneous local heat transfer coefficients, H, particle packing, $(1-\varepsilon')$, circumferential particle velocity, V_c and temperature, T_c. *(Continued overleaf.)*

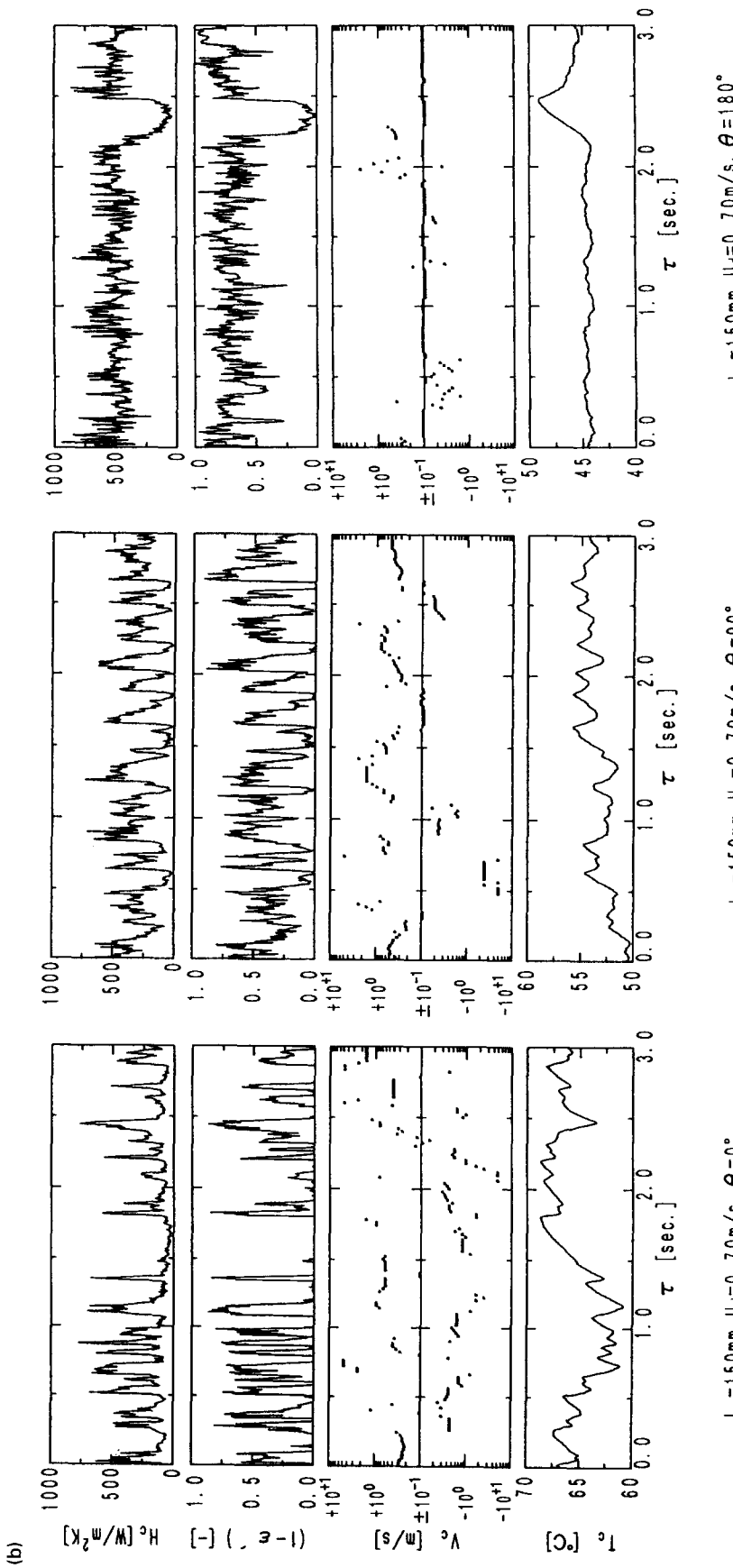

Fig. 6. *(Continued.)*

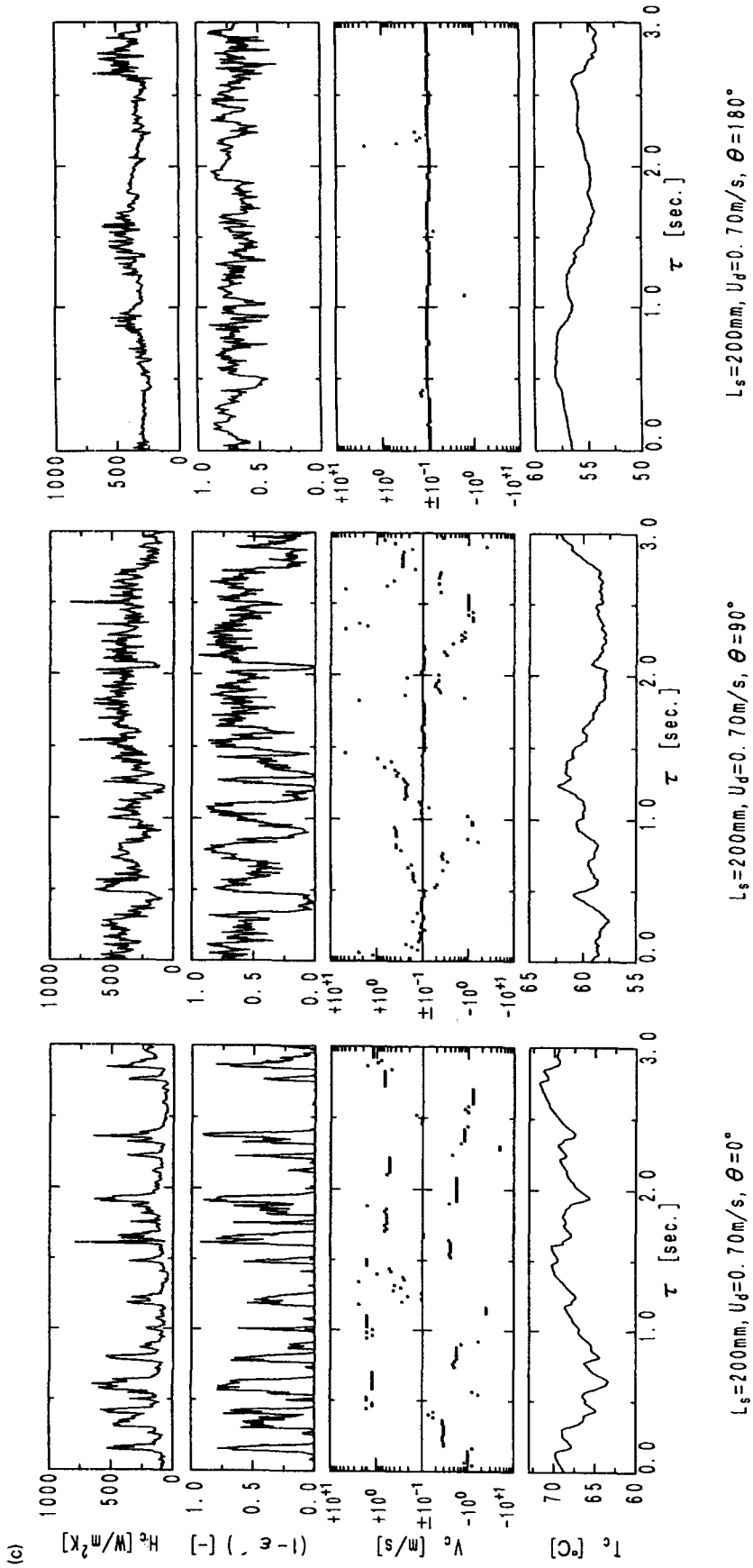

Fig. 6. (*Continued.*)

ation of each particle-packet contact was shorter than 0.15 s. At $\theta = 90°$, the contact time was slightly longer when compared with the case of $\theta = 0°$; however, the particle packing during contact was generally low and therefore the increase of the heat transfer coefficients caused by the particle contact was relatively small. At this angular position, the measured particle velocity showed that the greater part of the contacting particle-packets was falling down along the periphery of the tube. At $\theta = 180°$, some particles were frequently coming into contact with the surface, and an unusual fluctuation of the heat transfer coefficient could sometimes be observed. A typical example of the fluctuation is shown at $\tau = 0.1$ s, when the heat transfer coefficient becomes momentarily very high although the corresponding particle packing seems to be low. This phenomenon is considered to be caused by collisions of particles falling onto the heat transfer surface, which have been blown up above the heat transfer tube by bubbles bursting in the expanded bed surface.

For L_s of 150 mm, the frequency of the particle-packet contacts, their contact times and their particle packings were large compared with the cases of $L_s = 100$ mm. Particularly, at $\theta = 180°$, some particles were always making contact with the surface, the particle sliding velocities were small, and the amplitudes of the fluctuating heat transfer coefficients were also relatively small.

For L_s of 200 mm, the frequency of the particle contacts became high when compared with that of $L_s = 100$ and 150 mm. But at $\theta = 0°$, the contact time of each particle-packet seemed to be similar to the case of $L_s = 100$ mm. At $\theta = 180°$, the amplitudes of fluctuating heat transfer coefficients and the particle velocities were small, and the process, in which the heat transfer coefficient decreased very slowly, like the relaxation process of transient heat conduction, could sometimes be observed.

In order to investigate the particle movement on the tube surface, the measured particle velocities at each angular position were separately averaged by distinguishing the velocities between the positive and negative directions. This conditional averaging method gives the following summarized qualitative results.

For the present experimental conditions, these conditionally averaged velocities did not exceed 1.5 m s^{-1} and their circumferential distributions always became maximum at $\theta = 0°$.

On the upper side of the tube ($\theta > 90°$) excluding $\theta = 180°$, particles that were sliding down on the tube surface were dominant, and the velocities became larger as the particles were more distant from the top of tube. For $L_s = 200$ mm, the present method sometimes could not give the accurate particle velocity because so many particles were always coming into contact with the upper surface of the tube. The general trends of the obtained velocities on the upper locations for $L_s = 200$ mm showed that the particle velocities were low.

On the lower half ($\theta < 90°$) of the tube excluding $\theta = 0°$, the particles that were sliding up along the tube surface were dominant. But for $L_s = 100$ mm and $U_d = 0.5$ and 0.7 m s^{-1}, the sliding-down particles could be observed as frequently as the sliding-up particles.

The time fraction of particle contact and the particle packing

The normalized output, V_p, of the optical probe system corresponding to an N of 0.5 was used as the threshold value distinguishing particle contact from no particle contact. The time fractions, R_p of the periods of particle contact and the normalized particle packings, $(1-\varepsilon')_p$, averaged during particle contact, being distinguished by the above mentioned threshold value, are shown in Fig. 7. The general trends of the distributions of R_p and $(1-\varepsilon')_p$ are changed corresponding to the relative locations between the average expanded bed surface and the instrumented tube. R_p is low at the lower surface of the tube and becomes high at the upper surface. With the exception of $L_s = 100$ mm, the trends of the distribution of $(1-\varepsilon')_p$ are similar to those for R_p. In the cases of $L_s = 150$ and 200 mm as well as the case of $U_d = 1.1$ m s^{-1} for $L_s = 100$ mm, R_p is almost 100% at $\theta \geqslant 135°$, where $(1-\varepsilon')_p$ becomes maximum, but its maximum value does not exceed 0.75. In the case of $L_s = 200$ mm, when the heat transfer tube was immersed in the expanded bed, the distribution of $(1-\varepsilon')_p$ and R_p for the different U_d is relatively similar except for the slightly higher distribution for U_d of 0.5 m s^{-1}.

Conditionally averaged local heat transfer coefficients

Figure 8 shows the distributions of the three kinds of time-averaged local heat transfer coefficients, H_p, H_b and H_a, which were obtained from H by averaging over the periods during particle contact, during no particle contact, and the total time including both periods respectively. The distributions only at U_d of 0.7 m s^{-1} for L_s of 100, 150 and 200 mm are shown in Fig. 8. When R_p became higher than 90%, H_b was not plotted because the number of the averaged data seemed to be too small to make the correct averaging.

In Fig. 8, the difference between the average local heat transfer coefficients, H_p and H_b, caused by the particle contact was made very clear. With the exception of the cases of $U_d = 0.5$ and 0.7 m s^{-1} for $L_s = 100$ mm, H_p was more than twice H_b. The difference in heat transfer characteristics resulting from the differences of the tube locations relative to the expanded bed surface was also made clear. The total time-averaged local heat transfer coefficient H_a is nearly equal to H_p at the upper area of the tube, where R_p is large, with the exception of the case of U_d lower than 1.1 m s^{-1} for L_s of 100 mm. On the lower side, even for the case of $L_s = 200$ mm (when the difference between H_a

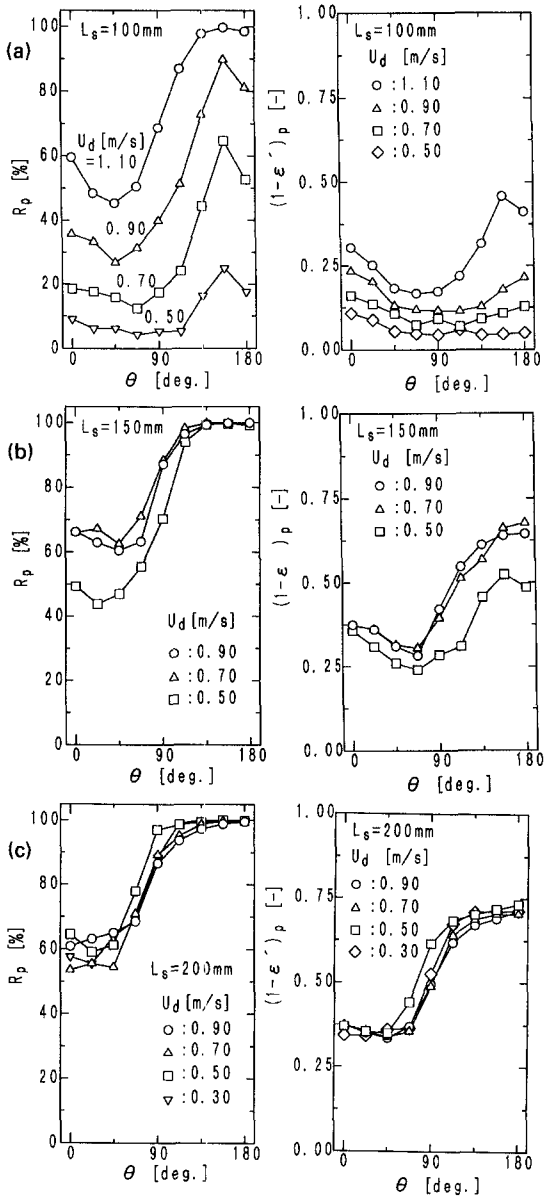

Fig. 7. Distributions of time fraction, R_p, of period during particle contact and average particle packing, $(1-\varepsilon')_{p'}$, during particle contact around tube.

and H_p is the smallest), the overall average heat transfer coefficient, H_a, does not exceed about 75% of H_p.

In Fig. 9, for all the present experimental conditions, the average local Nusselt number Nu_p in the period during particle contact, calculated from H_p in Fig. 8, is plotted against the average local particle packing, $(1-\varepsilon')_p$ in the period during particle contact shown in Fig. 7. The solid line in Fig. 9 was obtained by the least square approximation using all the data, excluding the cases of $\theta > 90°$ for only $L_s = 200$ mm, and was given by the following equation.

$$Nu_p = 10.1(1-\varepsilon')_p^{0.882}. \quad (3)$$

Here the correlation coefficient of the least-square approximation is 0.994 and the dotted lines indicate a deviation of $\pm 15\%$ from equation (3). The results shown in Fig. 9 indicate that, except for the case of $\theta > 90°$ for $L_s = 200$ mm, the average local Nusselt numbers during particle contact are closely correlated with the average local particle packing, and the correlation can be closely approximated by the single exponential equation of $(1-\varepsilon')_p$, in spite of the differences of the static bed heights, superficial gas velocities and angular positions of the tube.

Dyrness *et al.* [6] considered that the average heat transfer coefficients around the tube in the splash zone of the fluidized bed were correlated with a linear function of the average particle packing around the tube. But Visser and Valk's heat transfer model [10] for the immersed surface in a fluidized bed gives the exponent two divided by three for the base of particle packing $(1-\varepsilon)^{2/3}$.

Decker and Glicksman [11] proposed a model of heat transfer in a fluidized bed of spherical particles with a relatively large diameter for which the particle thermal time constant was larger than the particle residence time. When the contribution of gas convection is negligible, their model gives $Nu_p = 12$. Their model for the emulsion is considered to give the Nusselt number corresponding to the present case at $(1-\varepsilon')_p = 1$. Therefore, their Nusselt number is about 20% higher than the present one, as shown in Fig. 9. The thermal time constant [11] of the particle used in the experiment is about 0.4 s. The conditional average particle velocities at the bottom of the tube range from 1.5 m s^{-1} to 0.9 m s^{-1}. Considering the fluctuating instantaneous heat transfer coefficients shown in Fig. 6 and their dissimilarity to the relaxation process of transient heat conduction, it seems to be possible that the particle thermal time constant is much larger than the particle residence time, to say the least, at the lower side of the tube or in the case of small particle packing during contact with the surface. On the other hand, in the case of $\theta > 90°$ for $L_s = 200$ mm, as mentioned above, the particles near the top of the tube are almost at rest and once they move away from the top, start to slowly slide down along the tube surface, therefore the particle residence time is longer and the heat transfer coefficients become lower.

The deviations from the correlation with the maximum value of 15% shown in Fig. 9 can be considered to result from the effects of factors other than particle packing, such as the velocities of the particle movement and the interstitial gas flow adjacent to the tube surface. In the present experimental results, those factors other than particle packing do not explicitly seem to have significant effects on the average heat transfer coefficient during particle contact. The effects of those factors on heat transfer will be studied in the future to further clarify the mechanisms of fluidized bed heat transfer.

In Fig. 10, the average Nusselt numbers, calculated by the circumferential averaging of the time-average

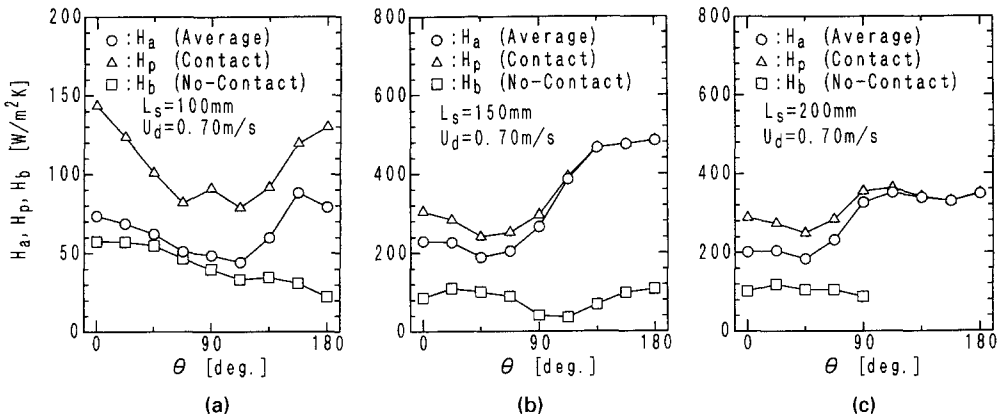

Fig. 8. Distributions of time-average local heat transfer coefficients, H_a, H_p and H_b, around tube.

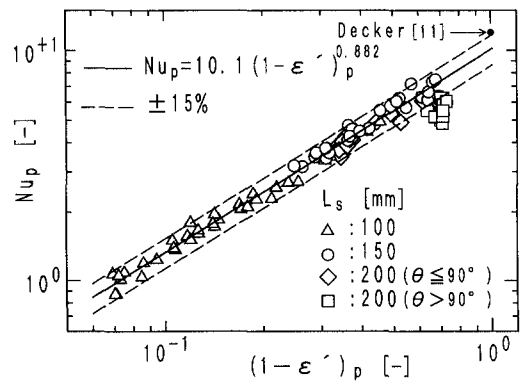

Fig. 9. Relation between time-average local Nusselt number, Nu_p, during particle contact and normalized time-average local particle packing $(1-\varepsilon')_p$.

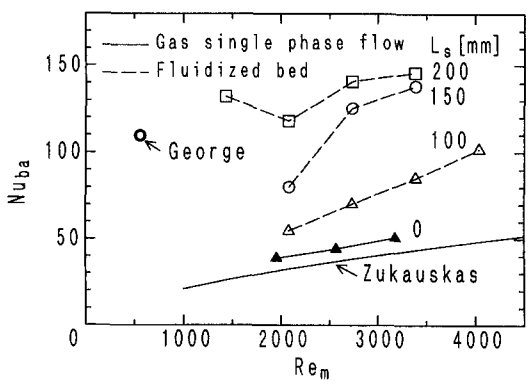

Fig. 10. Circumferential average of time-average local Nusselt number, Nu_{ba}, during no particle contact around tube.

heat transfer coefficients, H_b, in the period during no particle contact indicated in Fig. 7, are plotted against the Reynolds numbers, Re_m. Re_m was defined by the particle diameter and the maximum gas velocity through the tube bundle. The results for the single-phase gas flow calculated from the empirical correlation equation given by Zukauskas [12] are plotted for comparison. The present results for single-phase gas flow measured using the present fluidized bed experimental apparatus without particles are also plotted.

The results obtained by Zukauskas are the average Nusselt numbers for a tube bundle with ten rows. The present single-phase gas results, corresponding to the average values for the second row, give a distribution parallel to the Zukauskas' results but 10% higher. The reason why the present results give slightly higher Nusselt numbers than Zukauskas' result might be that strong turbulence was caused by the distributor plate being located relatively near the tubes. The correlations obtained by Zukauskas give about 10% higher Nusselt numbers for tubes at the 4th and 5th row than the average value for the 10-row bundle, as shown in Fig. 10. The highest turbulence intensities are at the 4th and 5th row among the tube bundle.

The average Nusselt numbers Nu_b during no particle contact in the fluidized bed are larger than those for the single-phase gas flow. This trend becomes more noticeable as the static bed height, L_s, and the superficial gas velocity, U_0, (Reynolds number) increase. In the case of L_s = 200 mm in which the tube is immersed in the expanded bed, the relation between Nu_b and Re_m seems to be roughly similar to that of the single-phase gas flow. As shown in Fig. 10, George's result obtained for an immersed tube in a bed with 1 mm diameter particles seems to be an extension of the present relation between Nu_b and Re_m for L_s = 200 mm.

The increase of the average heat transfer coefficients during no particle contact, being compared with those for the single-phase gas flow, is thought to be caused both by the high turbulence in the gas flow resulting from the existence of particles by the renewal of the thermal boundary layer on the tube with particle contact.

6. CONCLUSIONS

The instantaneous local heat transfer coefficients and the particle behavior around the heat transfer

tube in a fluidized bed were simultaneously measured at the same location. When the heat transfer tube was located near the expanded bed surface, the particle contact heat transfer augmentation mechanisms were quantitatively studied. Conditional averaging statistical analyses were carried out by distinguishing the measured results between the periods of particle contact and no particle contact. The main results obtained are summarized as follows.

1. For all the present experimental conditions except the angular locations $\theta > 90°$ for L_s of 200 mm, the average local Nusselt numbers in the period during particle contact can be closely correlated with a function of the average local particle packing during particle contact. The correlation equation is given by equation (3).

2. The overall average Nusselt numbers around the tube during no particle contact become higher than those for the corresponding single-phase gas flow and they increase as the static bed height and superficial gas velocity increase. This fact means that the heat transfer rates in the period during no particle contact also depend on the particle packing in the period during particle contact at the same location.

Acknowledgements—The authors wish to thank Mr M. Okada for assisting with the measurements using the optical fiber probe.

REFERENCES

1. N. A. Decker, Heat transfer to horizontal tubes in large particle gas fluidized beds, Ph.D. Thesis, Massachusetts Institute of Technology, Cambridge MA (1983).
2. T. Khan and R. Turton, The measurement of instantaneous heat transfer coefficients around the circumference of a tube immersed in a high temperature fluidized bed, *Int. J. Heat Mass Transfer* **35,** 3397–3406 (1992).
3. H. Ishiguro, H. Nariai and K. Ichikawa, Unsteady fluidization structure and heat transfer mechanism around a horizontal circular cylinder in a gas–solid fluidized bed, *Trans. JSME, B* **57-537,** 1772–1779 (1993).
4. A. H. George, Instantaneous local heat transfer coefficients and related frequency spectra for a horizontal cylinder in a high temperature fluidized bed, *Int. J. Heat Mass Transfer*, **36,** 337–345 (1993).
5. H. S. Li, R. Z. Qian, W. D. Huang and K. J. Bi, An investigation on instantaneous local heat transfer coefficients in high-temperature fluidized beds—2. Statistical analysis, *Int. J. Heat Mass Transfer* **36,** 4397–4406 (1993).
6. A. Dyrness, L. R. Glicksman and T. Yule, Heat transfer in the splash zone of a bubbling fluidized bed, *Int. J. Heat Mass Transfer* **35,** 847–860 (1992).
7. M. Miyamoto, Y. Katoh and Y. Idei, Heat transfer and particle behavior around horizontal tube bundle in gas fluidized bed, *Trans. JSME, B* **59-560,** 1291–1297 (1993).
8. J. V. Beck, B. Blackwell and C. R. S. Clair, *Inverse Heat Conduction*, Wiley-Interscience, New York (1985).
9. M. Ishida, T. Shirai and A. Nishiwaki, Measurement of the velocity and direction of flow of solid particles in a fluidized bed, *Powder Technol.* **27,** 1–7 (1980).
10. G. Visser and M. Valk, The porosity in a fluidized bed heat transfer model, *Int. J. Heat Mass Transfer* **36,** 627–632 (1993).
11. N. Decker and L. R. Glicksman, Heat transfer in large particle fluidized beds, *Int. J. Heat Mass Transfer* **26,** 1307–1320 (1983).
12. A. Zukauskas, Heat transfer from tubes in crossflow. In *Advances in Heat Transfer*, Vol. 8 (Edited by J. P. Hartnett and T. F. Irvin), pp. 93–160. Academic Press, New York (1972).